On the Feasibility of Automated Mechanical Ventilation Control Through EIT

Henry F. J. Tregidgo, Michael G. Crabb, Andrew L. Hazel, and William R. B. Lionheart

Abstract*—*Objective: **This paper aims to demonstrate the feasibility of coupling electrical impedance tomography (EIT) with models of lung function in order to recover parameters and inform mechanical ventilation control.** ***Methods:*** **A compartmental ordinary differential equation model of lung function is coupled to simulations of EIT, assuming accurate modeling and movement tracking, to generate time series values of bulk conductivity. These values are differentiated and normalized against the total air volume flux to recover regional volumes and flows. These ventilation distributions are used to recover regional resistance and elastance properties of the lung. Linear control theory is used to demonstrate how these parameters may be used to generate a patient-specific pressure mode control.** ***Results:*** **Ventilation distributions are shown to be recoverable, with Euclidean norm errors in air flow below 9% and volume below 3%. The parameters are also shown to be recoverable, although errors are higher for resistance values than elastance. The control constructed is shown to have minimal H^1 seminorm resulting in bounded magnitudes and minimal gradients.** ***Conclusion:*** **The recovery of regional ventilation distributions and lung parameters is feasible with the use of EIT. These parameters may then be used in model based control schemes to provide patient-specific care.** ***Significance:*** **For pulmonary-intensive-care patients mechanical ventilation is a life saving intervention, requiring careful calibration of pressure settings. Both magnitudes and gradients of pressure can contribute to ventilator induced lung injury. Retrieving regional lung parameters allows the design of patient-specific ventilator controls to reduce injury.**

***Index Terms*—Electrical impedance tomography, model predictive control, mechanical ventilation, lung protective ventilation.**

I. Introduction

MECHANICAL ventilation strategies play a vital role for the treatment of patients in respiratory intensive care units. The use of mechanical ventilation can be life saving for patients in multiple situations, for example acute lung injuries such as acute respiratory distress syndrome (*ARDS*) [1], [2] or acute complications to chronic conditions such as chronic obstructive pulmonary disease (*COPD*). However, increased stress on lung tissue can cause ventilator induced lung injury (*VILI*) [3].

The risk of VILI increases in the more severe forms of ARDS, where the lung is smaller and more inhomogeneous [4], [5]. In these circumstances, given the low lung volume the currently recommended tidal volume (6 mL/Kg ideal body weight) can result in excessive lung strain (tidal volume/end-expiratory lung volume ratio) and consequent risk of volutrauma. In addition, during inspiration lung inhomogeneity can cause important rises in alveolar pressure between neighbouring lung regions at different level of inflation (stress risers). Inhomogeneity is considered a significant factor contributing to VILI and these two factors explain why despite using lung protective ventilation (*LPV*) significant VILI can still occur [6], [7].

Two related approaches to developing LPV strategies are to regulate both the volume of air flow and driving pressures experienced by the patient. Larger tidal volumes increase the variations in pressure between full inhalation and exhalation. One recent study [8] has shown that the magnitude of this driving pressure is strongly adversely linked with the mortality rate of patients. Additionally, modelling the process of airway opening has revealed that inducing gradients of pressure within opening airways can cause damage [9].

In addition to monitoring variations in pressure, it is also important to set the end expiratory pressure level correctly. Because airway collapse or recruitment can cause drastic changes in the ventilation pattern of the lungs [10], the positive end expiratory pressure (*PEEP*) is set as the minimum pressure applied during expiration to keep airways open. There are multiple ways to determine an optimal PEEP setting [11], but generally a recruitment manoeuvre is performed, followed by PEEP titration using measures such as lung compliance or blood gas composition to determine when an acceptable pressure has been found [12]. These approaches, by necessity, rely upon taking measurements that can be easily accessed from the bedside, making it difficult to take into account regional variations in the structure and health of the lungs.

Mechanical ventilation can result in some lung lobes being over-distended, causing damage, while others are only partly recruited [13]. This, combined with regional variations in perfusion, can cause areas of alveolar dead space which do not assist in gas transfer [14]. It is therefore desirable to have some form of bedside imaging to recover regional ventilation distributions and inform ventilation strategies. However, radiation concerns [15]

Manuscript received August 2, 2017; revised November 10, 2017 and December 22, 2017; accepted January 20, 2018. Date of publication February 23, 2018; date of current version October 18, 2018. This work was supported by EPSRC under Grant EP/L019108/1 Robust Repeatable Respiratory Monitoring with EIT. The work of W. R. B. Lionheart was supported by a Royal Society Wolfson Research Merit Award. *(Corresponding author: Henry F. J. Tregidgo.)*

Henry F. J. Tregidgo is with the School of Mathematics, University of Manchester, Manchester M13 9PL, U.K. (e-mail: henry.tregidgo@manchester.ac.uk).

M. G. Crabb, A. L. Hazel, and W. R. B. Lionheart are with the School of Mathematics, University of Manchester, Manchester.

Digital Object Identifier 10.1109/TBME.2018.2798812

limit the frequency with which computerised tomography *(CT)* may be used for routine monitoring, while magnetic resonance imaging *(MRI)* requires expensive tracers to accurately monitor air flow [16]. Additionally, neither CT nor MRI is practical at the bedside.

One proposed solution is the use of EIT. It has been shown that air content of the lungs causes a high contrast in the conductivity levels of tissue [17] and so time series of EIT reconstructions can be used to monitor the regional ventilation of the lungs [18]. This has enabled clinicians to begin incorporating EIT into patient care, and techniques are being examined for such purposes as monitoring lung fluid content [19], improving PEEP titration [20] and verifying the efficacy of pressure controls [21].

These techniques have the advantage that EIT has high temporal resolution and is safe to use at the bedside for extended periods [22]. This has resulted in the proposal of using EIT for regional monitoring of lung function during recruitment manoeuvres. In their paper Costa *et al.* [23] describe a method for recovering a regional measure of lung function they name *pixel compliance*, which is a measure of impedance change between PEEP and plateau pressure. This measure is useful in estimating alveolar collapse and hyperdistension on a regional basis to determine an optimal PEEP level. However, it is not clear how to use pixel compliance to model the response of the lung to pressure controls directly. For this reason we examine the feasibility of converting high frequency regional ventilation information into objective measures of lung function based on widely known lung models. Once parameters have been recovered we examine their utility in optimising ventilation strategies for the patient.

To incorporate EIT into the control of mechanical ventilators it is necessary to examine existing control procedures. Modern ventilators rely on both user input and feedback control techniques from control theory. Chatburn lists a hierarchy for the levels of user input and feedback control in his review of computer control systems [24]. The lowest level in this hierarchy is *set-point* control, in which the user defines a set pressure to be experienced by the patient. Due to the interaction between the patient's lung and the ventilator, the applied pressures may not be the same as those experienced by the patient's airways, so the ventilator uses measurements of the airway pressure as feedback to adjust the applied pressures accordingly.

A more advanced approach in Chatburn's hierarchy is to allow the computer to modify this pressure set-point based on optimising mathematical models of lung function in a scheme known as *optimal control*. One example of such a model is given by Li and Haddad [25], where they track changes in pressure, volume flows and states between breathing periods for a simulated lung system. They then use a linear compartmental reference model for the lungs to adapt their pressure control using a *repetitive model predictive control* scheme. However, model based approaches are limited by the availability of patient specific model parameters. This motivates our feasibility study on incorporating patient-specific parameters from EIT into a model based control scheme.

Using patient-specific lung parameters and standard techniques in control theory, it is possible to directly calculate pressure controls for a target state while minimising the so-called H^1 semi-norm associated with the Sobolev space $W^{1,2}$ [26], [27]. By modelling the response of the lung to a given pressure control profile and using the result as a target for control, we demonstrate that a new patient-specific profile may be generated. Such an approach ensures that the magnitude of the new pressures remain bounded and the time gradients of pressure are minimised without changing the resulting ventilation state of the patient. We demonstrate that this is possible for a model of lung function in which regional parameters are recoverable from EIT. This is a necessary first step in the development of true patient-specific mechanical ventilation controls.

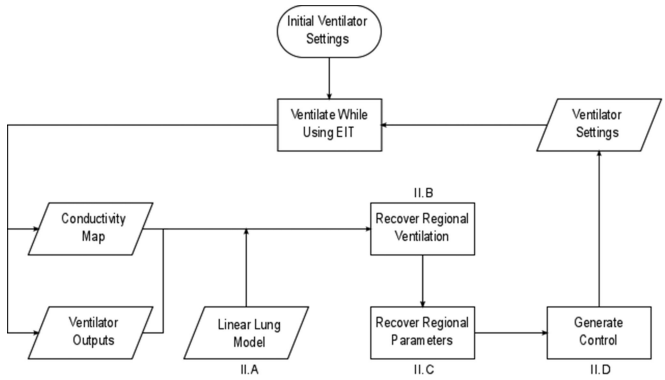

Fig. 1. Flowchart showing a proposed procedural workflow for implementing EIT guided control of mechanical ventilation, including section numbers for implementations of post processing steps.

We present a feasibility study of techniques to detect regional airflow from imaging, recover regional ventilation parameters and modify pressure controls to improve them with respect to the H^1 semi-norm. We perform tests using the observed relationships between electrical conductivity and air volume, as well as the noise properties of EIT reconstructions. These techniques may be adapted to work with other imaging modalities so long as they can provide information on the regional distribution of air within the lungs with a high temporal resolution. A preliminary version of this work has already been reported [28].

II. Methods

To determine the feasibility of EIT guided control of mechanical ventilation, the workflow shown in Fig. 1 is examined. In Section II-A a linear ordinary differential equation (*ODE*) compartmental model of the lungs is outlined. This model uses the mechanical parameters *resistance* and *elastance* defined for different regions of the lung, which can be used to determine when ventilator settings are acceptable [29]. In Section II-B the recovery of regional ventilation profiles by coupling EIT conductivity reconstructions and ventilator data during normal ventilation is described. In Section II-C the recovery of mechanical parameters from the regional ventilation profiles is outlined. In Section II-D techniques from linear control theory are used to generate a pressure control specifically designed to have bounded magnitudes and minimal time gradients. Once the control procedure has finished the process of recovering ventilation and parameters begins again during a new phase of normal ventilation.

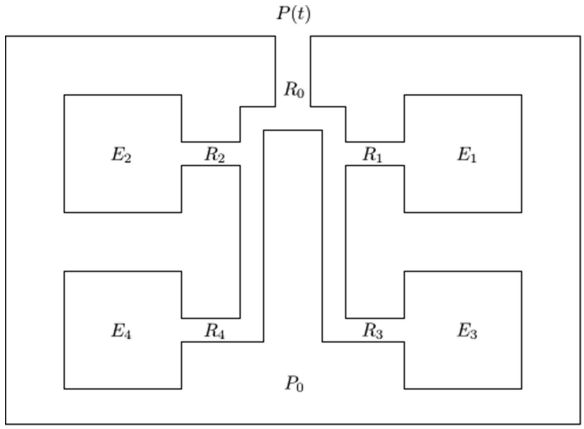

Fig. 2. Compartment layout for ODE model. Compartments are labeled in the order top right, top left, bottom right, bottom left to align with an extruded chest model used to simulate EIT reconstruction.

This paper provides an initial feasibility study of the workflow Fig. 1 outlined in Sections II-A to II-D rather than any specific EIT reconstruction or segmentation scheme. In a clinical setting bulk parameters would have to be recovered from the imaging modality, and in the case of EIT there would first be an initial step of segmenting the image and obtaining a representative conductivity value from each segment. In the present feasibility study this is simulated by generating conductivity time series for each compartment, using a homogenisation rule, and correlated noise is generated by performing difference EIT on voltage measurements with added noise. This method, described in detail in Section II-E, generates time series with errors following a distribution likely to be found in clinical measurements.

A. Linear ODE Lung Model

A linear compartmental ODE model is used to test the workflow in Fig. 1. Such models have been a standard method for understanding lung function for over 60 years [30] and have been well studied [31]. There is also evidence for the accuracy of these models as similar models have been used to provide boundary conditions in computational fluid dynamics simulations of the lungs [32].

Equations in this section model air as an incompressible fluid passing through a central airway into four compartments under the action of a pressure difference as shown in Fig. 2. These compartments have been assigned to upper and lower lung regions on left and right sides of thorax as described in Section II-E. Four compartments have been specified as a demonstrative example due to dyadic branching tree structure of the lungs and to simplify the modelling process in Section II-E. Section IV-A examines further how these compartments may be aligned with physiologically meaningful divisions of the lung.

In the model, pressure drops occur as air passes through the central airway and the airways leading into each compartment under the action of airway resistance. Each airway has its own resistance parameter denoted by R_i, where i denotes the number assigned to the compartment each airway leads to and R_0 refers to the central airway, or tracheal, resistance. Once airway pressure drops have been accounted for the pressure difference between air within each compartment and the pleural pressure outside the lungs is counteracted by the elastance of each compartment denoted by E_i.

Denote the volume of air in each compartment at time t as the continuous scalar function $v_i(t)$. By conservation of mass the volume flow at the top of the airway is taken to be the sum of the rates of change in each of these volumes. The difference between the driven pressure at time t, $P(t)$, and the pleural pressure P_0 can be formulated as the equation

$$P(t) - P_0 = R_0 \sum_{j=1}^{4} \dot{v}_j(t) + R_i \dot{v}_i(t) + E_i v_i(t), \qquad (1)$$

as described in [33, chapter 7]. Equation (1) holds true for each of the compartments and can therefore be reformulated into a matrix ODE system.

Using bold notation to denote vectors, $\mathbf{v}(t)$ is defined to be a vector containing the air volumes $v_i(t)$, $\mathbf{p}(t)$ is a vector of pressure drops, $P(t) - P_0$, across the system and E and R are matrices with the structures

$$E = \begin{pmatrix} E_1 & 0 & 0 & 0 \\ 0 & E_2 & 0 & 0 \\ 0 & 0 & E_3 & 0 \\ 0 & 0 & 0 & E_4 \end{pmatrix},$$

$$R = \begin{pmatrix} R_1 + R_0 & R_0 & R_0 & R_0 \\ R_0 & R_2 + R_0 & R_0 & R_0 \\ R_0 & R_0 & R_3 + R_0 & R_0 \\ R_0 & R_0 & R_0 & R_4 + R_0 \end{pmatrix}. \qquad (2)$$

This allows eq. (1) to be reformulated as

$$R\dot{\mathbf{v}}(t) + E\mathbf{v}(t) = \mathbf{p}(t), \qquad (3)$$

which is then solved using a fourth order explicit Runge-Kutta method, allowing calculation of the system's response to smooth input pressure profiles.

B. Ventilation Monitoring from EIT

This section describes the recovery of the ventilation distribution, i.e. compartmental flows and volumes for the models in Section II-A, from EIT images. EIT reconstruction generates time series of homogenised or effective conductivities σ_i, that are related to air volume v_i, for each compartment. It is demonstrated here that the recovery of interior flow and volumes can be reduced to differentiation of conductivity time series and fitting to the measured flow data at the ventilator. The case where compartmental volumes are known up to a Gaussian noise distribution is examined in [34, chapter 6].

In [21] and [35] it is shown that there is an approximate linear relationship between the effective electrical resistivity ρ_i, and *filling factor* F. Here ρ_i is approximated as the reciprocal of effective conductivity, $\rho_i \approx \frac{1}{\sigma_i}$, and F is defined as the ratio of air volume content to tissue volume. This results in a relationship of the form

$$v_i = \alpha V_i \rho_i + \beta, \qquad (4)$$

where V_i is the volume of lung tissue in compartment i, and α and β are constants independent of ρ_i. It is assumed that V_i can be determined from another imaging modality capable of determining regional air volumes. For example the Hounsfield unit values assigned to volume elements in a CT image are proportional to the tissue content of that element, allowing the volumes of air and tissue to be computed [36]. For the purposes of this study β is estimated by computing a linear fit of values from the equations used in Section II-E to generate conductivity maps.

Under the assumption of incompressibility the volume flow measured at the ventilator Q is equal to the sum of the compartmental flows. This allows α to be determined by performing a least squares fit on the equation

$$Q = \alpha \sum_i \frac{\mathrm{d}}{\mathrm{d}t}(V_i \rho_i) = \alpha \sum_i V_i \frac{\mathrm{d}}{\mathrm{d}t}\rho_i, \tag{5}$$

once the ρ_i have been differentiated. Differentiation amplifies the effects of noise so the time derivative of ρ_i is posed as the inversion of an integration operator to allow explicit regularisation of the solution [37]. This gives the equation

$$\frac{\mathrm{d}}{\mathrm{d}t}\tilde{\boldsymbol{\rho}}_{\boldsymbol{i}} = \arg\min_{\mathbf{u}} \|A\mathbf{u} - \boldsymbol{\rho}_{\boldsymbol{i}}\|^2 + \lambda_i \|L\mathbf{u}\|^2, \tag{6}$$

where $\boldsymbol{\rho}_{\boldsymbol{i}}$ is a time series vector containing the ρ_i values for multiple time samples, A is an integration matrix used in a data-fit term, in this case constructed using the composite trapezium rule, λ_i is a regularisation hyperparameter, L is a second order central difference operator used to enforce a level of smoothness on the solution and $\tilde{\boldsymbol{\rho}}_{\boldsymbol{i}}$ is a regularised approximation to the resistivity time series of the compartment.

The regularisation hyperparameters for each compartment are found using an L-curve method. L-curve methods aim to balance the data misfit with the regularisation penalty by plotting the resulting values of the residual and regularisation norms on a log-log plot. This graph has a characteristic L shape and the value of λ_i corresponding to the point of maximal negative curvature, or corner, is typically used due to the transition at this point between the two straight sections. Modified versions of the functions `cgsvd` and `l_curve` from the Regularization Tools Matlab toolbox [38] are used to choose the regularisation parameter for this problem automatically. In this case parameters within an interval correspond to points on the graph with negative curvature, producing a rounded corner. As such, λ_i is chosen to be the lower of the two values in this interval at points with half the maximum curvature. This is to emphasise the data-fit for the use of reconstructed flows in parameter estimation.

Once the regularisation parameter has been found for each compartment a Tikhonov regularised inverse can be found for the problem in eq. (6) allowing the derivative to be computed quickly. The result is a smooth approximation to the time derivative of the electrical resistivity in a given compartment. These derivatives are then summed and normalised against the volume flow measured at the mouth to give a measure of regional flow. Integrating these values with respect to time then gives a regularised approximation to the resistivity time series of the compartment removing measurement noise to aid in later parameter estimation. This time series can then be converted into an approximation for the air volume within a compartment.

C. Ventilation Parameters from Regional Flows

Once the smoothed flows and volumes have been estimated using the methods in Section II-B, these can be used in a parameter estimation problem to find the mechanical ventilation parameters E_i and R_i for each compartment and airway. As in Section II-A the governing equations for this inversion can be derived from eq. (1). However, unlike in eq. (3), the parameters of resistance and elastance are treated as the dependent variables while the values of compartmental flow and resistance are known parameters. This allows the system to be reformulated as a single matrix multiplication $M\mathbf{x} = \mathbf{P}$, in which the matrix M is composed of copies of the time series values of flows and volumes while entries of the target vector $\mathbf{x}$ are the desired parameters and $\mathbf{P}$ contains copies of the pressure series.

Using over-tilde notation to denote quantities which have been recovered in Section II-B, denote $\tilde{\mathbf{Q}}$ as a vector of length S containing the sum of the smoothed compartmental flows, and build matrices $\tilde{M}_i$, with dimension $S \times 2$, and vectors $\tilde{\mathbf{P}}$ of length S in the form

$$\tilde{M}_i = \begin{pmatrix} \tilde{v}_i(t_1) & \dot{\tilde{v}}_i(t_1) \\ \vdots & \vdots \\ \tilde{v}_i(t_S) & \dot{\tilde{v}}_i(t_S) \end{pmatrix} \qquad \tilde{\mathbf{P}} = \begin{pmatrix} P(t_1) - P_0 \\ \vdots \\ P(t_S) - P_0 \end{pmatrix}, \tag{7}$$

with S denoting the number of time samples. Using $\tilde{\mathbf{Q}}$, $\tilde{M}_i$ and $\tilde{\mathbf{P}}$ and block matrix notation, eq. (1) can be reformulated as a $4S \times 9$ overdetermined system $M\mathbf{x} = \mathbf{P}$ with the form

$$\begin{pmatrix} \tilde{\mathbf{Q}} & \tilde{M}_1 & 0 & 0 & 0 \\ \tilde{\mathbf{Q}} & 0 & \tilde{M}_2 & 0 & 0 \\ \tilde{\mathbf{Q}} & 0 & 0 & \tilde{M}_3 & 0 \\ \tilde{\mathbf{Q}} & 0 & 0 & 0 & \tilde{M}_4 \end{pmatrix} \begin{pmatrix} R_0 \\ E_1 \\ R_1 \\ E_2 \\ R_2 \\ E_3 \\ R_3 \\ E_4 \\ R_4 \end{pmatrix} = \begin{pmatrix} \tilde{\mathbf{P}} \\ \tilde{\mathbf{P}} \\ \tilde{\mathbf{P}} \\ \tilde{\mathbf{P}} \end{pmatrix}, \tag{8}$$

which can be solved by a Moore-Penrose generalised inverse to give a least squares solution

$$\tilde{\mathbf{x}} = (M^T M)^{-1} M^T \mathbf{P}. \tag{9}$$

D. Ventilation Optimisation from Control Theory

This section describes techniques for modifying the pressure set point of a ventilator, using parameters recoverable via the methods in Sections II-A to II-C. The control theory concepts in this section are classical linear control theory techniques which are taken from [26] and [27, Part 1].

The approach examined in this paper stems from the controllability of the ODE model described in Section II-A. A controllable linear system of ODEs

$$\dot{\mathbf{y}} = A\mathbf{y} + B\mathbf{u}, \tag{10}$$

can be steered from any state $\mathbf{y_0}$ to any other state $\mathbf{y_T}$ in time T by a control $\mathbf{u}$. In this general case $\mathbf{y}$ is an n-dimensional function, A is an $n \times n$ state space matrix, B is an $n \times m$ state space matrix and $\mathbf{u}$ is an m-dimensional control function.

Applying the definition of controllability to the lung models from Section II-A would appear to imply that regions of lung could be controlled independently. However, in practice the controls produced to do this would violate constraints on both pressure and air flow. This coupled with the simplicity of the lung models used prohibits the design of full feedback control schemes from these methods. Instead this section describes a simple model predictive control scheme to test the feasibility of incorporating parameters from bedside imaging into ventilator control. This scheme uses parameters, recoverable through the methods in Section II-C during a normal ventilation period, to optimise a prototype pressure mode control for a given initial condition and time period before returning to normal ventilation as outlined in Fig. 1. The resulting control has improved magnitudes and gradients of pressure, while steering the ODE model to the same end state as the initial prototype.

The possibility of optimising a prototype pressure profile stems from the fact that the controls corresponding to given initial conditions, target states and time constraints are not unique. However, there exist closed form solutions providing the controls that are minimal in a given norm. The control that has minimal L^2 norm,

$$\|u\|_{L^2} = \left(\int_0^T |u(s)|^2 \mathrm{d}s \right)^{\frac{1}{2}}, \tag{11}$$

is specified at every time s as

$$\mathbf{u}(s) = -B^* \exp\{(T-s)A^*\} Q_T^{-1} (\exp\{TA\}\mathbf{y_0} - \mathbf{y_T}), \tag{12}$$

where Q_T is a Gramian matrix [27, Prop 1.1]. Therefore, if the system in eq. (10) is controllable, the result of ventilating with a prototype profile can be simulated and eq. (12) can be used to generate an equivalent profile with minimal pressure magnitudes.

Before the control in eq. (12) may be used, the controllability of the system must be confirmed. This is done by examining the Kalman controllability matrix

$$K = [B|AB|\cdots|A^{n-1}B]. \tag{13}$$

A necessary and sufficient condition for the system in eq. (10) to be controllable is for matrix K to have rank n, where n is the length of the vector $\mathbf{y}$ [26], or in this case the number of separate compartments in the model. To determine if the lung system is controllable eq. (3) is reformulated as

$$\dot{\mathbf{v}} = -R^{-1}E\mathbf{v} + R^{-1}\mathbf{b}(P(t) - P_0), \tag{14}$$

where $\mathbf{b}$ is a vector of ones and the matrix *K* is formed from eq. (13), using

$$A = -R^{-1}E, \qquad B = R^{-1}\mathbf{b}. \tag{15}$$

The rank of K is then calculated to determine if the system is controllable. The circumstances which result in a loss of controllability, along with methods for treating these cases, are discussed in Section IV-C.

Once controllability has been determined the control pressures are generated. To improve numerical stability this is done using the basis of eigenvectors. Therefore the first step is computing the eigenpairs for the matrix $-R^{-1}E$. It can be proven that the eigenvalues for this matrix are negative and have a full set of linearly independent eigenvectors, giving the equation

$$-R^{-1}E = UDU^{-1} \tag{16}$$

where the columns of U are the eigenvectors and D is a diagonal matrix of eigenvalues. Properties of these eigenpairs are discussed further in Section IV-C.

The required Gramian Q_T is then computed as

$$\begin{aligned} Q_T &:= U \left[\int_0^T \exp\{Dr\} U^{-1} \mathbf{b}\mathbf{b}^* U^{-*} \exp\{Dr\} \mathrm{d}r \right] U^*, \\ &= U \bar{Q}_T U^*, \end{aligned} \tag{17}$$

and the required exponentials are computed as

$$e^{-R^{-1}E(T-s)} = U e^{D(T-s)} U^{-1}. \tag{18}$$

These are combined using eq. (12) to provide a control pressure $\mathbf{u}$ of the form

$$\mathbf{u}(s) = -\mathbf{b}^* U^{-*} e^{D(T-s)} \bar{Q}_T^{-1} (e^{DT} U^{-1} \mathbf{v_0} - U^{-1} \mathbf{v_T}), \tag{19}$$

where $\mathbf{v_0}$ and $\mathbf{v_T}$ are the initial and target values of $\mathbf{v}$.

These result can also be generalised such that if the system in eq. (10) is controllable then so is the system

$$\begin{aligned} \begin{pmatrix} \dot{\mathbf{y}} \\ \dot{\mathbf{u}} \end{pmatrix} &= \begin{pmatrix} A & B \\ 0 & 0 \end{pmatrix} \begin{pmatrix} \mathbf{y} \\ \mathbf{u} \end{pmatrix} + \begin{pmatrix} 0 \\ I \end{pmatrix} \mathbf{w}, \\ \dot{\bar{\mathbf{y}}} &= \bar{A}\bar{\mathbf{y}} + \bar{B}\mathbf{w} \end{aligned} \tag{20}$$

where I indicates the appropriate identity matrix. This result follows from construction of the corresponding Kalman controllability matrix, which will have full rank if K has full rank, and allows a control to be found that minimises the H^1 seminorm,

$$|u|_{H^1} = \left(\int_0^T |\dot{u}(s)|^2 \mathrm{d}s \right)^{\frac{1}{2}}. \tag{21}$$

This means that a pressure profile can be constructed that takes a linearised model of the lungs to a specified state, at a given pressure with minimised jumps and oscillations.

The methods shown in eq. (17) to eq. (19) may be generalised for the system in eq. (20). The eigenvalues for this system are the same as those for eq. (10) with the addition of a zero eigenvalue. Therefore the eigenpairs must be updated to include a zero eigenvalue with corresponding eigenvector and the vector $\mathbf{b}$ must be adjusted to correspond to the new system. By doing this and following the procedure above, the formula in eq. (19) produces the derivative of the control pressure and can be integrated numerically to provide a *minimised H^1 pressure profile*.

Additionally, as both the initial and final pressures are specified in this formulation, it is possible to relate this to the full

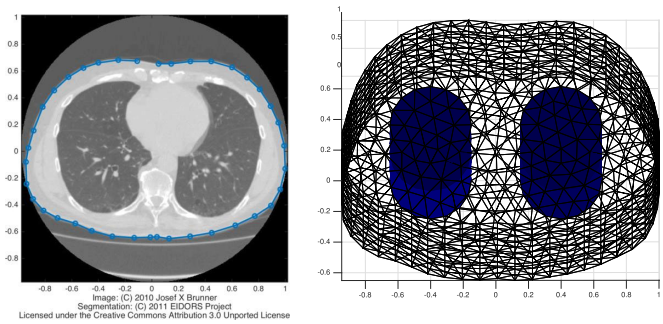

Fig. 3. Human adult male thorax CT outline (left) and extruded mesh used for reconstruction aggregation (right).

H^1 norm. As the gradients of this control are minimised, the pressures must be close to a linear function between the two pressures measured in the H^1 semi-norm. In fact, using the Poincaré-Fredrichs inequality, it can be proved that the H^1 norm of this difference is bounded by a constant times the difference between the original pressure and the same linear function. The constant is monotonically increasing with both the control time period and improvement between original and minimised profiles as measured in the H^1 semi-norm. This implies that for large enough improvements in gradients the full H^1 norm of the new control will also be improved, resulting in both lower pressures magnitudes and minimal gradients.

E. Simulating Conductivity Time Series with Noise

This section describes the process of generating time series values of bulk conductivity. This involves the generation of a finite element (FE) model of the thorax including segmented compartments representing the lungs. This FE mesh is then used to produce correlated noise through EIT to simulate best case reconstructions.

Volume time series values from the equations in Section II-A are converted to conductivity time series using the equations described by Nopp in [39]. These equations model alveoli as cubes and include components for blood, cellular membrane, endothelial and epithelial cells, and extracellular and intracellular fluids. Given the conductivity time series, correlated noise is generated by reconstructing voltage measurement noise directly through EIT. This gives a reasonable approximation to the level of noise produced under the assumptions that the shape of a patient's thorax can be modelled and tracked accurately through the course of ventilation [40], electrode positioning and impedance is modelled accurately [41] and the noise in each of the voltage measurements follow independent, identical distributions.

Before generating the conductivity time series, FE meshes of the thorax geometry are built using Netgen [42] to extrude the boundary contour of the adult male chest CT shown on the left in Fig. 3. Three meshes are produced including the coarse mesh shown in Fig. 3 as well as a fine and ultra-fine mesh. These are composed of 10K, 341K and 1.03M volume elements respectively and each contain four cylindrical inclusions. For the purposes of this feasibility study and to simplify the mesh generation process the cylinders represent the four compartments in the lung model from Section II-A. The fine and ultra-fine meshes include 4 rings of 16 electrodes embedded onto the outer thorax shape in order to simulate EIT as described later in this section.

In order to set the compartmental conductivity time series using the Nopp equations, the frequency of EIT current injection, taken here as 100 kHz, the filling factor and the ratio of lung tissue conductivity to background conductivity in each lung compartment cylinder must be specified. To calibrate the ratio of conductivities between lung and background tissues, the values given in [43] are used providing a ratio of 0.125 at full inhalation. The mid inhalation conductivities are generated by normalising the Nopp conductivity values for max inhalation, at $F = 4$ [39], to 0.125 and then calculating the normalised conductivities expected if the lung model were held at the median ventilation pressure.

Simulated EIT voltage measurements and conductivity reconstructions are produced using modified code from EIDORS version 3.8 [44]. The electrodes are indexed from 1 to 64, where electrodes in the top ring are numbered from 1 to 16 and the further 3 rings are indexed beginning at 17, 33 and 49 respectively. EIT is simulated with pairwise current driven at 0.1mA and voltages are measured on pairwise electrodes both with a skip of 23 so that current is driven and measurements are recorded across rings. The voltages are computed on the ultra-fine mesh through a piecewise linear FE method using the complete electrode model [45]. Noise values are generated using a normal distribution with a signal to noise ratio of $\|\phi\|/\|\epsilon\| = 100$ where ϕ is a vector of measured voltage differences and ϵ is the vector of noise values. Measured in decibels this equates to a 40 dB signal, which is significantly worse than the practical upper range of accuracy in EIT measurements of approximately 100 dB [46]. The errors in conductivity caused by these voltage noise values are calculated using the EIDORS function `inv_solve_diff_GN_one_step`. This reconstructs conductivity using a single Gauss-Newton step with a Jacobian calculated using the fine mesh of the domain. The values from this inversion are mapped to the coarse mesh to aggregate the reconstruction and reduce the dimensionality of the problem. The reconstructed conductivity values are then aggregated into four compartmental noise values by taking a volume weighted average within the regions of interest. These four averaged values are then added to the Nopp generated values to give a noisy sampled time series of conductivities.

III. Results

The techniques described in Sections II-A to II-E were used to test the feasibility of the procedure shown in Fig. 1. Firstly the ventilation distribution for the model described in Section II-A were generated for a period of 30 s with an assumed EIT data acquisition rate of 20 frames per second, giving 600 equispaced time steps. The parameters used, shown in Table I, were chosen to be of a similar magnitude to those provided in [33] and to ensure that the parameters could be recovered and that the ODE system is controllable, which will

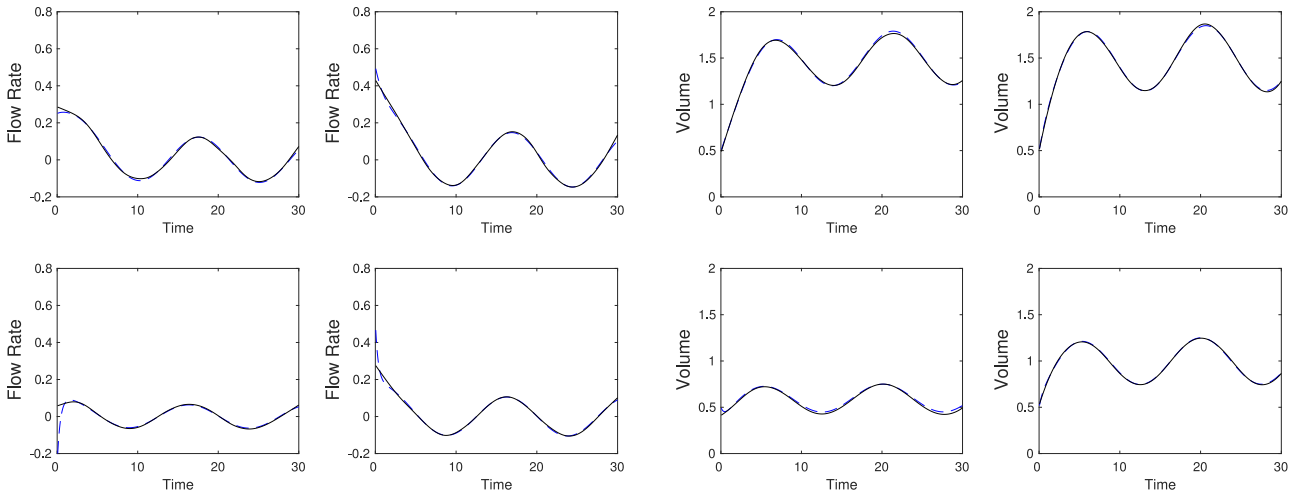

Fig. 4. Graphs comparing the simulated and recovered flows and volumes in each compartment. True simulated values are shown as a dashed blue line, while reconstructed values are a solid black line. Flows are shown on the left and volumes are shown on the right.

TABLE I
MODEL PARAMETERS

	Elastance (Pressure/Volume)	Resistance (Pressure × Time/Volume)
Compartment 1	10	10
Compartment 2	10	20
Compartment 3	15	5
Compartment 4	25	10
Trachea	-	5

be discussed further in Section IV-C. These parameters are given in arbitrary units of pressure per volume for elastance and pressure per volume multiplied by time for resistance as all quantities were normalised to achieve tidal breathing variations consistent with filling factor values given in the literature [39]. The input pressure profile for ventilation followed a sinusoidal pattern with values chosen such that the most compliant compartments would reach full exhalation and inhalation filling factor values if held at minimum or maximum pressures respectively. The initial conditions were chosen such that each compartment started with a filling factor of 1, simulating a lung collapsed beyond normal exhalation being reinflated by mechanical ventilation. The resulting volumes were used to calculate a time series of compartmental conductivity values.

EIT reconstruction of noise voltages were performed for each time step and volume averaged noise values added to the conductivity time series as described in Section II-E. The techniques from Sections II-B to II-C were then used to find recovered ventilation distribution and parameters. This process was repeated 1000 times with new draws from a normally distributed pseudorandom number generator to test robustness to noise.

To test the feasibility of the techniques in Section II-D an H^1 minimisation procedure for a PEEP step was simulated. First the response of the system to a sinusoidal pressure profile, oscillating at 18 breaths per minute, was calculated. A step up in PEEP during the sixth breath was generated by a smoothed Heaviside function. This *original profile* was chosen to demonstrate the behaviour of the H^1 minimisation process on pressure profiles while ensuring the stability of the fourth order explicit Runge-Kutta method used in simulation. A control was then generated to produce the same jump in pressures and volumes over the course of three breaths. This was performed using the true ventilation parameters to demonstrate the properties of the control under optimal conditions.

All timings presented are from calculations performed on a 2.8 GHz Intel Core i7-3840QM processor with 16GB 1.6 GHz DDR3 RAM, running code written for MATLAB_R2015a. For comparison the difference EIT reconstructions performed took an average of 2.4 ms per frame.

A. Ventilation Monitoring

In each case, the recovered flows and volumes were qualitatively close to the original simulated values as shown in Fig. 4. However, differences can be seen at the edges of the flow graphs in Fig. 4. These errors and their positioning in the time series flow pattern highlights one weakness in this approach to recovering flow parameters. By using Tikhonov regularisation and a high regularisation parameter additional smoothness is enforced on the flows which may obscure features that are highly localised or occur at higher frequencies. In this case the initial transient behaviour of the flows inflating compartments from a partially collapsed state is dampened during the initial frames.

This effect is demonstrated further by examining the norms of errors in the flow recovery. Table II shows the Euclidean norms of the error in recovered flows, $\|\dot{v}_i - \dot{y}_i\|_2$, taken as a percentage of the same norm applied to the simulated flow $\|\dot{y}_i\|_2$, where $\dot{y}_i$ is the simulated flow for compartment i. Both the mean error and standard deviation (*STD*) are shown for the full flow and the flow limited to exclude the first 2.5 s that are dominated by the transient behaviour.

This effect is not as pronounced for the volume reconstructions, as shown by minor vertical offsets in the volume graphs in Fig. 4. This is due to the fact that the flows are integrated

TABLE II
FLOW RECOVERY RELATIVE ERRORS

Comp. No.	Mean (Full)	STD (Full)	Mean (Limited)	STD (Limited)
1	6.46%	1.02%	6.77%	1.65%
2	8.53%	1.72%	7.33%	1.99%
3	16.58%	0.80%	6.15%	1.49%
4	49.37%	1.48%	8.39%	1.69%

TABLE III
VOLUME RECOVERY RELATIVE ERRORS

Comp. No.	Min	Max	Mean	STD
1	0.46%	4.42%	1.32%	0.58%
2	0.47%	4.30%	1.34%	0.59%
3	0.49%	4.81%	1.36%	0.64%
4	1.41%	5.51%	2.36%	0.57%

to produce the volumes, meaning that the L^2 error values are equivalent to a rescaled evaluation of the data fit term in eq. (6). As the data fit term is an explicit part of the differentiation step it is expected that the errors in volume recovery should be smaller than those for flow reconstruction.

Similarly Table III shows the same Euclidean norm error percentages as applied to the volumes recovered. As expected from the qualitative behaviour in Fig. 4, the errors shown in these tables are higher and more varied for the flow recovery than for the volume recovery.

The computation time for these flows is more encouraging. Although the initial differentiation step took 0.52 seconds (s) this dropped to between 113 and 198 ms for all subsequent runs. Similarly the time taken to normalise the differentiated values, converting to volumes and flows, was initially 49 ms but dropped to between 3.8 and 6.9 ms. This implies that clinicians could be presented with visual representations of a period of regional ventilation within approximately 0.2 s of post processing time.

B. Parameter Recovery

In each test the reconstructed volumes and flows were used to generate the system matrix shown in eq. (8), which in turn was used to generate recovered ventilation parameters through eq. (9). Both the simulated parameters and the distribution of the recovered parameters are shown in Fig. 5.

Elastance values were generally recovered much more accurately than compartmental resistance values, while the resistance values were harder to recover in compartments with higher elastance. In order to compare the recovery of these different parameters a time constant was calculated for each compartment as the total recovered series resistance leading to a compartment, including tracheal resistance, divided by the recovered compartmental elastance. These time parameters have clinical relevance, as time constant ratios of flow rate to lung volume can be used as a measure of lung health [47]. The distribution of these recovered time constants is shown in Table IV. In each compartment the value the mean overestimation of this time

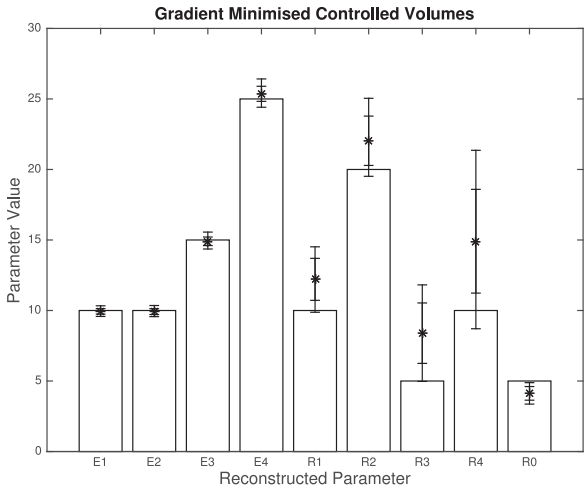

Fig. 5. Chart showing the true simulated values (bars) and the distribution of their recovered values (lines). The vertical lines are marked at the minimum, maximum and mean values recovered as well as points two standard deviations from the mean.

TABLE IV
TIME CONSTANT RECOVERY ERRORS

Comp. No.	True Value	Mean	Error	STD(%)
1	1.50	1.64	0.14	3.68%
2	2.50	2.64	0.14	2.83%
3	0.67	0.84	0.17	8.56%
4	0.60	0.75	0.15	10.52%

constant was between 0.14–0.17 s with a standard deviation in the error of less than 11%. While values were not recovered perfectly, the near constant bias in time constant recovery may allow the compartments relative health to be compared.

The low error ranges for elastance recovery are also encouraging as they may be easily converted to the more common measure of compliance, currently used for guiding recruitment manoeuvres. These regional measures were again recoverable within a short time, taking between 0.3 ms and 6.6 ms to compute after the flows had been recovered. This implies that the parameter recovery technique is a natural choice for extending the volume and flow recovery in a clinical setting.

C. Control

Volumes and flows were generated under the action of the sinusoidal pressure profile described above with a simulated increase in pressure at $t = 20$ s using the techniques in Section II-A. The pressure patterns for first 5 and last 2 breaths were retained to be used in the new pressure profile. The ventilator pressure and compartmental volumes taken at $t = 15$ s as initial condition for H^1 control, while the pressure and volumes taken at $t = 25$ s were taken as a target for steering.

Fig. 6 shows both the original smoothed PEEP step as described above and the minimised H^1 pressure profile for this increase in PEEP. Fig. 7 shows the responses of the system to both PEEP increases.

As expected the initial five and final two breaths proceed exactly the same under the action of both pressure profiles. The

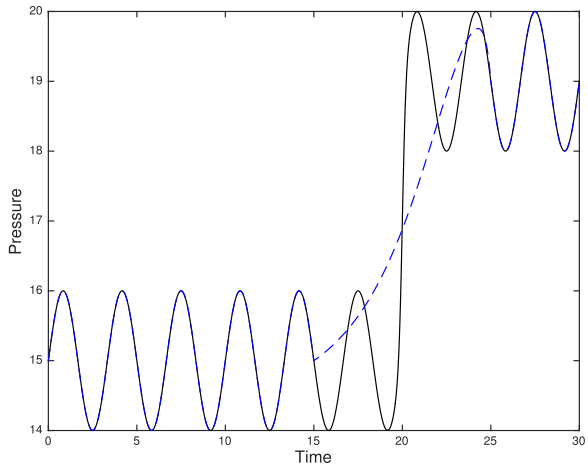

Fig. 6. Original (solid line) and minimised H^1 (dotted line) pressure profile including an increase in PEEP level.

only differences are found during the controlled section. In the controlled case, the rate of pressure increase is slower, while the flow spikes visible for the original pressure profile are smoothed out reducing stress on the lungs.

The process of predicting a flow for the given pressure profile, obtaining initial and target conditions, generating a control and recombining to give a minimised H^1 pressure profile took 10.9 ms. This demonstrates that by combining regional information with control theory, it may be possible to derive patient specific pressure controls that attain the same results as classical techniques while reducing risk factors.

IV. Discussion

A. Ventilation Modelling and Recovery

In the interests of demonstrating the feasibility of this workflow the ODE ventilation model has been used for forward modelling, parameter recovery and control, this is an example of an *inverse crime*. Inverse crimes occur when the same model is used to both generate and invert simulated data [48] leading to better reconstructions with simulated data as opposed to measured data. This improvement in reconstructions justifies the model re-use in this instance. The post processing techniques in sections Sections II-B to II-D cannot be feasible if they do not work with the reconstructions provided in this manner. Where possible, other inverse crimes have been avoided, for example using the Nopp formulas to generate conductivity values rather than assuming a perfect linear relationship, or using different mesh refinements for voltage generation, calculation of the Jacobian and reconstruction.

Use of the ODE model illustrated in Fig. 2 is, in the authors' opinion, a reasonable simplification of the lung system for the purpose of recovering regional parameters. The structure of the lungs can be split into lobes and bronchopulmonary segments each supplied by a single branch in the bronchial tree mirroring the compartmental structure of the ODE. Segmentation of imaging down to at least lobe level has been achieved [49]–[51], raising the possibility of obtaining values for compartments in the ODE model corresponding to lung lobes. This motivates the choice of a four compartment model for our tests as each compartment can then correspond to a physiologically distinct region supplied by airways at the same bifurcation level of the lung's dyadic tree structure, where two lobes of the right lung are treated as one functional unit.

This model also allows the production of numeric and visual representations of the distribution of regional ventilation and of parameters such as regional elastance. These provide additional information on the degree of regional inhomogeneity present in the lung. As lung inhomogeneity is considered a risk factor for VILI [6], [7], this information could be of use to clinicians in understanding whether therapeutic intervention, such as recruitment manoeuvres, variation in PEEP levels or prone positioning, are effective at decreasing regional lung inhomogeneity and therefore increasing lung protection. Similarly this information could help identify when mechanical ventilation remains injurious and, in the more severe forms, lung rest and extracorporeal support should be sought as a way to achieve lung protection [52]. Nevertheless the qualitative fidelity of the ODE systems, and recovered parameters, compared to more complex models must be verified before implementation in a clinical setting.

Another source of difficulty with this model is the current trend in the EIT community to use what is known as 2.5D difference imaging. This is where reconstructions are performed using a single plane of electrodes modelled on an extruded 2D contour, ensuring the volume does not vary along the caudal-distal axis. To resolve physiologically meaningful compartments, and calibrate the recovered air volumes, 3D imaging must be performed [53] with some way of estimating a constant of integration between compartmental flows and volumes. As shown in Section II-B it is possible to obtain a constant of proportionality from time derivative information but obtaining true values of air volume requires more information. A first approximation to this may be acquired by taking 1 frame of absolute EIT, informed with mutual information from MRI or CT [54], followed by difference imaging. Hence, EIT noise distributions are modelled using difference imaging in this paper

B. Parameter Recovery

The ventilation parameters used in this paper are chosen to ensure the existence of a unique solution to the system in eq. (8). It can be proved that for periodic pressure profiles the system matrix has linearly independent columns so long as the parameter pairs (R_i, E_i) are not all multiples of each other. The proof relies on treating the non-zero sections of each matrix column as a function that can be Fourier decomposed. As many of these sections are constructed from volumes, they must be non-negative and have a non-trivial zero frequency component, which will not be present in the flow columns. Due to the structure of the matrix and the repeated presence of the top level flow, for the matrix to drop in rank the top level flow must be a linear multiple of each compartmental flow. Choosing compartments

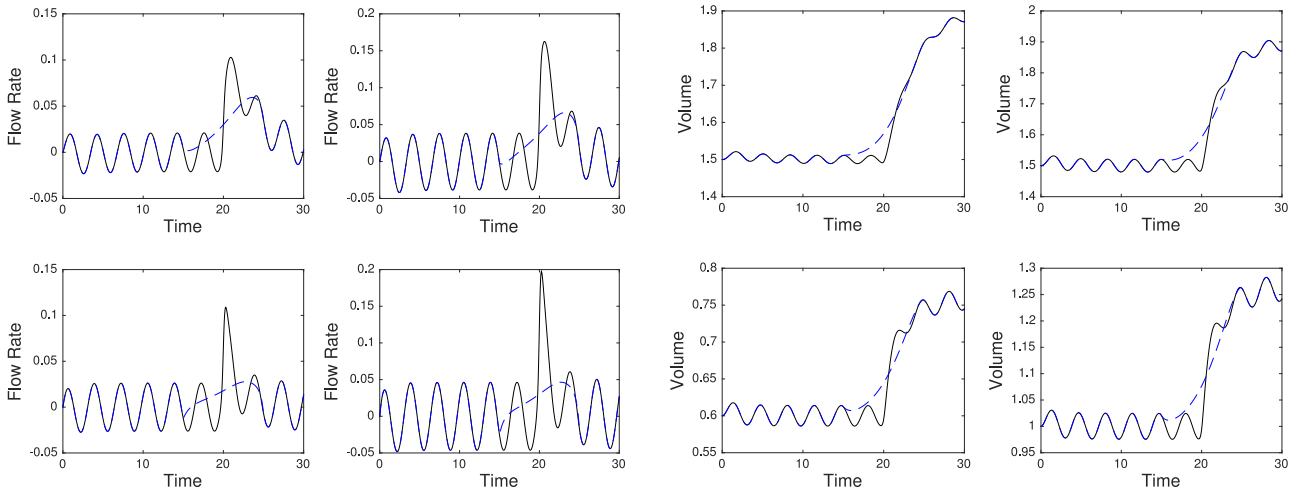

Fig. 7. Flow (left) and volume (right) responses of the system to both a step increase in pressure (solid lines) and minimised H^1 control pressure (dashed line)

to have linearly independent sets of R and E ensures recoverable parameters.

This means that, although there is not always a unique solution to eq. (8), it is always possible to find the regional elastance values and obtain ratios between resistances in different compartments, using any clinically acceptable, periodic pressure profile. It also means that in the most dangerous situations for lung health, where successive compartments are out of phase with each other, there will always be a unique least squares solution.

Once the system matrix is built from reconstructed flows, the problem in eq. (8) becomes a total least squares problem (*TLS*). TLS problems arise where a least squares solution is needed to a system with unknown errors in both the measured data vector and the system matrix [55]. Unconstrained solutions to this type of problem can be computed using singular value decompositions. However, applying these techniques to the problem in eq. (8) was found to produce larger errors in reconstructed values. This is possibly due to the block structure and sparsity of the system matrix in this case. It is possible that the use of constrained total least squares (*CTLS*) techniques [56], [57] may improve the parameter recovery. However, as it is unclear how the errors in the matrix would be distributed, implementation of these techniques was deemed beyond the scope of this paper.

C. Control

The first step in designing a control using techniques in Section II-D is to test if the system is controllable by taking the rank of the matrix K shown in eq. (13). Computing the rank of a matrix is an ill-posed operation especially when the dimension is increased by having large numbers of compartments. Instead it is more stable to examine the equivalent matrix

$$[\hat{\mathbf{b}}|D\hat{\mathbf{b}}|\cdots|D^{n-1}\hat{\mathbf{b}}], \tag{22}$$

where $\hat{\mathbf{b}}$ is the pressure transfer vector in the basis of eigenvectors and D is a diagonal matrix of eigenvalues for the system [26]. From this it can be seen that the rank will drop in the case of a repeated eigenvalue in D or a zero entry in $\hat{\mathbf{b}}$. In the case of zero tracheal resistance this only happens when compartmental parameter pairs (R_i, E_i) are multiples of each other. The presence of tracheal resistance introduces a rank one perturbation to the eigenvalues of the system making such a determination more complex. Rank one perturbation theory allows conditions to be defined on the separation of eigenvalues in the unperturbed system to guarantee distinct eigenvalues for the perturbed system [58]. Using these methods it can be shown that a drop in rank only occurs when the parameters for different compartments are close to being multiples of each other [59, Chapter 4]. This causes these compartments to be ventilated in phase with each other allowing them to be treated as one larger compartment to be controlled. Therefore, in these cases, the ODE model can be reformulated to reduce the number of compartments and the same minimisation techniques can be used on the new system.

While the controllability of these systems is encouraging it does not imply that a feasible control can be created to reach any desired ventilation state directly. Unphysical changes in pressure, including large negative pressures, were observed when targeting unstable states of ventilation. This is due to the lack of constraints on the pressure in this formulation of control theory. While the H^1 minimisation process produces a smoother pressure profile than any that attains the same result, more advanced constrained control or optimisation is needed to compute the best control for any given situation.

A similar argument may be made for problems with automated feedback control. Decreasing the time between initial condition and target can result in high temporal gradients in pressure so completely controlling the volumes from one time step to the next is currently infeasible. Similarly extending the time period used for control resulted in sections of constant pressure for increasing lengths of time. These were followed by the same waveform in order to attain the required target state. This raises the concept of a natural time scale for changes to be

applied. Ideally an optimisation procedure will be developed to find best states and time periods to steer towards.

It is also important to note that control in this case uses a linearisation of a non-linear system. As airways open during a control procedure, the compliance of under-recruited compartments will change [29]. This will make the control less accurate the longer process takes and the further the target is from the initial conditions. However, it still offers potential improvements in cases such as recruitment manoeuvres.

V. Conclusion

The care of mechanically ventilated patients benefits greatly from improvements in both monitoring techniques and systematic methods of correctly setting the ventilator. Current ventilation strategies rely on global measures of lung function or the average responses of large groups. Safe, robust and repeatable imaging techniques available at the bedside raise the possibility of tailoring care to regional lung changes and the associated changes in a patient's requirements.

We investigate three post processing procedures for EIT to improve the ability of the imaging modality to usefully inform clinicians. Through these procedures both regional ventilation and ventilation parameters may be estimated for a linearisation of the lung system. This parameter estimation can be attained without modifying the pressure profile used for ventilation, reducing the negative impacts of monitoring.

As well as informing care this allows construction of modifications to existing recruitment manoeuvres through control theory. These minimal H^1 controls are designed to attain the same results while reducing the risks of high gradients in pressure or large flow rates.

As the combined time for calculating volumes, parameters and controls is fractions of a second it is feasible to attempt personalised control of ventilation for mechanically ventilated patients through the use of EIT.

Acknowledgment

The authors would like to thank Luigi Camporota for many productive discussions on the requirements for effective monitoring in respiratory intensive care.

References

[1] V. Ranieri *et al.*, "Acute respiratory distress syndrome: The Berlin definition," *JAMA*, vol. 307, no. 23, pp. 2526–2533, 2012.
[2] G. Bellani *et al.*, "Epidemiology, patterns of care, and mortality for patients with acute respiratory distress syndrome in intensive care units in 50 countries," *JAMA*, vol. 315, no. 8, pp. 788–800, 2016.
[3] D. Dreyfuss and G. Saumon, "Ventilator-induced lung injury: Lessons from experimental studies," *Amer. J. Resp. Crit. Care*, vol. 157, no. 1, pp. 294–323, 1998.
[4] A. S. Slutsky and V. Ranieri, "Ventilator-induced lung injury," *New Eng. J. Med.*, vol. 369, no. 22, pp. 2126–2136, 2013.
[5] L. Gattinoni *et al.*, "The 'baby lung' became an adult," *Intensive Care Med.*, vol. 42, no. 5, pp. 663–673, 2016.
[6] P. P. Terragni *et al.*, "Tidal hyperinflation during low tidal volume ventilation in acute respiratory distress syndrome," *Amer. J. Resp. Crit. Care*, vol. 175, no. 2, pp. 160–166, 2007.
[7] M. Cressoni *et al.*, "Lung in homogeneities and time course of ventilator-induced mechanical injuries," *Anesthesiology*, vol. 123, no. 3, pp. 618–627, 2015.
[8] M. B. Amato *et al.*, "Driving pressure and survival in the acute respiratory distress syndrome," *New Eng. J. Med.*, vol. 372, no. 8, pp. 747–755, 2015.
[9] A. M. Bilek *et al.*, "Mechanisms of surface-tension-induced epithelial cell damage in a model of pulmonary airway reopening," *J. Appl. Physiol.*, vol. 94, no. 2, pp. 770–783, 2003.
[10] K. G. Hickling, "The pressure—volume curve is greatly modified by recruitment: a mathematical model of ARDS lungs," *Amer. J. Resp. Crit. Care*, vol. 158, no. 1, pp. 194–202, 1998.
[11] J. J. Rouby *et al.*, "Selecting the right level of positive end-expiratory pressure in patients with acute respiratory distress syndrome," *Amer. J. Resp. Crit. Care*, vol. 165, no. 8, pp. 1182–1186, 2002.
[12] T. Piraino, "Decremental PEEP titration: A step away from the table," *Respiratory care*, vol. 58, no. 5, pp. 886–888, 2013.
[13] S. R. Vieira *et al.*, "A scanographic assessment of pulmonary morphology in acute lung injury: Significance of the lower inflection point detected on the lung pressure—volume curve," *Amer. J. Resp. Crit. Care*, vol. 159, no. 5, pp. 1612–1623, 1999.
[14] T. J. Nuckton *et al.*, "Pulmonary dead-space fraction as a risk factor for death in the acute respiratory distress syndrome," *New Eng. J. Med.*, vol. 346, no. 17, pp. 1281–1286, 2002.
[15] M. K. Kalra *et al.*, "Strategies for CT radiation dose optimization," *Radiology*, vol. 230, no. 3, pp. 619–628, 2004.
[16] H. E. Möller *et al.*, "MRI of the lungs using hyperpolarized noble gases," *Magn. Resonance Med.*, vol. 47, no. 6, pp. 1029–1051, 2002.
[17] H. Luepschen *et al.*, "Protective ventilation using electrical impedance tomography," *Physiol. Meas.*, vol. 28, no. 7, pp. S247–S260, 2007.
[18] N. Kerrouche *et al.*, "Time series of EIT chest images using singular value decomposition and Fourier transform," *Physiol. Meas.*, vol. 22, no. 1, pp. 147–157, 2001.
[19] A. Adler *et al.*, "Monitoring changes in lung air and liquid volumes with Electrical Impedance Tomography," *J. Appl. Physiol.*, vol. 83, no. 5, pp. 1762–1767, 1997.
[20] Z. Zhao *et al.*, "PEEP titration guided by ventilation homogeneity: A feasibility study using electrical impedance tomography," *Crit. Care*, vol. 14, no. 1, 2010.
[21] C. J. Roth *et al.*, "Correlation between alveolar ventilation and electrical properties of lung parenchyma," *Physiol. Meas.*, vol. 36, no. 6, pp. 1211–1226, 2015.
[22] W. R. Lionheart *et al.*, "Generalized optimal current patterns and electrical safety in EIT," *Physiol. Meas.*, vol. 22, no. 1, pp. 85–90, 2001.
[23] E. L. Costa *et al.*, "Bedside estimation of recruitable alveolar collapse and hyperdistension by electrical impedance tomography," *Intensive Care Med.*, vol. 35, no. 6, pp. 1132–1137, 2009.
[24] R. L. Chatburn, "Compute control of mechanical ventilation," *Respiratory care*, vol. 49, no. 5, pp. 507–517, 2004.
[25] H. Li and W. M. Haddad, "Model predictive control for a multicompartment respiratory system," *IEEE Trans. Control Syst. Technol.*, vol. 21, no. 5, pp. 1988–1995, Sep. 2013.
[26] R. E. Kalman, "Mathematical description of linear dynamical systems," *SIAM J. Appl. Math., Series A, Control*, vol. 1, no. 2, pp. 152–192, 1963.
[27] J. Zabczyk, *Mathematical Control Theory: An Introduction*. Berlin, Germany: Springer Sci. & Bus. Media, 2009.
[28] H. F. J. Tregidgo *et al.*, "A mathematical control theory approach to EIT guided mechanical ventilation," in *Proc. 16th Int. Conf. Biomed. Appl. EIT*, 2015, p. 96.
[29] K. G. Hickling, "Best compliance during a decremental, but not incremental, positive end-expiratory pressure trial is related to open-lung positive end-expiratory pressure: A mathematical model of acute respiratory distress syndrome lungs," *Amer. J. Resp. Crit. Care*, vol. 163, no. 1, pp. 69–78, 2001.
[30] A. Otis *et al.*, "Mechanical Factors in Distribution of Pulmonary Ventliation," *J. Appl. Physiol.*, vol. 8, no. 4, pp. 427–443, 1956.
[31] B. Maury, *The respiratory system in equations*. Berlin, Germany: Springer Science & Business Media, 2013.
[32] M. Ismail *et al.*, "Coupled and reduced dimensional modeling of respiratory mechanics during spontaneous breathing," *Int. J. Numerical Methods Biomed. Eng.*, vol. 29, no. 11, pp. 1285–1305, 2013.
[33] J. Bates, *Lung Mechanics: An Inverse Modeling Approach*. Cambridge, U.K.: Cambridge Univ. Press, 2009.
[34] M. G. Crabb, "EIT reconstruction algorithms for respiratory intensive care," Ph.D. dissertation, Univ. of Manchester, Manchester U.K., 2014.

[35] S. Trudelle *et al.*, "Electrical Impedance Tomography: Characterization of in-vitro performance," in *Proc. Eng. Med. Biol. Soc., 1995., IEEE 17th Annu. Conf.*, 1995, vol. 1, pp. 563–564.
[36] L. Gattinoni *et al.*, "The role of CT-scan studies for the diagnosis and therapy of acute respiratory distress syndrome," *Clinics Chest Med.*, vol. 27, no. 4, pp. 559–570, 2006.
[37] J. Cullum, "Numerical differentiation and regularization," *SIAM J. Numer. Anal.*, vol. 8, no. 2, pp. 254–265, 1971.
[38] P. C. Hansen, "Regularization tools version 4.0 for matlab 7.3," *Numer. Algorithms*, vol. 46, no. 2, pp. 189–194, 2007.
[39] P. Nopp *et al.*, " Model for the dielectric properties of human lung tissue against frequency and air content," *Med. Biol. Eng. Comput.*, vol. 35, no. 6, pp. 695–702, 1997.
[40] B. Grychtol *et al.*, "Impact of model shape mismatch on reconstruction quality in Electrical Impedance Tomography," *IEEE Trans. Med. Imag.*, vol. 31, no. 9, pp. 1754–1760, 2012.
[41] A. Boyle and A. Adler, "The impact of electrode area, contact impedance and boundary shape on EIT images," *Physiol. Meas.*, vol. 32, no. 7, pp. 745–754, 2011.
[42] J. Schöberl, "NETGEN - An Advancing Front 2D/3D-Mesh Generator Based On Abstract Rules," *Comput. Visual. Sci.*, vol. 1, pp. 41–52, 1997. [Online]. Available: http://www.hpfem.jku.at
[43] A. Adler *et al.*, "Impedance imaging of lung ventilation: Do we need to account for chest expansion?" *IEEE Trans. Biomed. Eng.*, vol. 43, no. 4, pp. 414–420, 1996.
[44] A. Adler and W. R. Lionheart, "Uses and abuses of EIDORS: An extensible software base for EIT," *Physiol. Meas.*, vol. 27, no. 5, pp. S25–S42, 2006.
[45] K.-S. Cheng *et al.*, "Electrode models for electric current computed tomography," *IEEE Trans. Biomed. Eng.*, vol. 36, no. 9, pp. 918–924, 1989.
[46] R. D. Cook *et al.*, "ACT3: A high-speed, high-precision electrical impedance tomograph," *IEEE Trans. Biomed. Eng.*, vol. 41, no. 8, pp. 713–722, 1994.
[47] N. Al-Rawas *et al.*, "Expiratory time constant for determinations of plateau pressure, respiratory system compliance, and total resistance," *Crit. Care*, vol. 17, no. 1, p. R23, 2013.
[48] A. Wirgin, "The inverse crime," preprint math-ph/0401050, 2004. [Online]. Available: https://arxiv.org/abs/math-ph/0401050
[49] J. Tschirren *et al.*, "Airway segmentation framework for clinical environments," in *Proc. 2nd Int. Workshop Pulmonary Image Anal.*, 2009, pp. 227–238.
[50] S. Montesantos *et al.*, "Airway morphology from high resolution computed tomography in healthy subjects and patients with moderate persistent asthma," *Anatomical Rec.*, vol. 296, no. 6, pp. 852–866, 2013.
[51] J. Fleming *et al.*, "A technique for determination of lung outline and regional lung air volume distribution from computed tomography," *J. Aerosol Med. Pulmonary Drug Del.*, vol. 27, no. 1, pp. 35–42, 2014.
[52] L. Gattinoni and M. Quintel, "How ARDS should be treated," *Crit. Care*, vol. 20, no. 1, p. 86, 2016.
[53] W. R. Lionheart, "Uniqueness, shape, and dimension in EIT," *Ann. NY Acad. Sci.*, vol. 873, no. 1, pp. 466–471, 1999.
[54] M. Crabb *et al.*, "Mutual information as a measure of image quality for 3D dynamic lung imaging with EIT," *Physiol. Meas.*, vol. 35, no. 5, pp. 863–879, 2014.
[55] G. H. Golub and C. F. Van Loan, "An analysis of the total least squares problem," *SIAM J. Numerical Anal.*, vol. 17, no. 6, pp. 883–893, 1980.
[56] T. J. Abatzoglou *et al.*, "The constrained total least squares technique and its applications to harmonic superresolution," *IEEE Trans. Signal Process.*, vol. 39, no. 5, pp. 1070–1087, May 1991.
[57] V. Z. Mesarović *et al.*, "Regularized constrained total least squares image restoration," *IEEE Trans. Image Process.*, vol. 4, no. 8, pp. 1096–1108, Aug. 1995.
[58] W. Kahan, "Spectra of nearly Hermitian matrices," *Proc. Amer. Math. Soc.*, vol. 48, no. 1, pp. 11–17, 1975.
[59] H. F. J. Tregidgo, "Inverse problems and control for lung dynamics," Ph.D. dissertation, Univ. Manchester, Manchester, U.K., 2017.